Understanding the Biosynthesis and Catalytic Activity of Pd, Pt, and Ag Nanoparticles in Hydrogenation and Suzuki Coupling Reactions at the Nano–Bio Interface

ARTICLE *in* THE JOURNAL OF PHYSICAL CHEMISTRY C · OCTOBER 2014

Impact Factor: 4.77 · DOI: 10.1021/jp508211t

6 AUTHORS, INCLUDING:

Sujoy K Das
Central Leather Research Institute
37 PUBLICATIONS **1,094** CITATIONS
SEE PROFILE

Thanusu Parandhaman
Central Leather Research Institute
3 PUBLICATIONS **37** CITATIONS
SEE PROFILE

Asit Baran Mandal
Central Leather Research Institute
360 PUBLICATIONS **3,202** CITATIONS
SEE PROFILE

Manabendra Mukherjee
Saha Institute of Nuclear Physics
98 PUBLICATIONS **876** CITATIONS
SEE PROFILE

THE JOURNAL OF PHYSICAL CHEMISTRY C

Article

pubs.acs.org/JPCC

Understanding the Biosynthesis and Catalytic Activity of Pd, Pt, and Ag Nanoparticles in Hydrogenation and Suzuki Coupling Reactions at the Nano−Bio Interface

Sujoy K. Das,*[,†] Thanusu Parandhaman,[†,#] Nagaraju Pentela,[‡,#] A. K. M. Maidul Islam,[∥] Asit Baran Mandal,*[,§] and Manabendra Mukherjee[⊥]

[†]Bioproduct Division, [‡]Polymer Division, and [§]Chemical Laboratory, Council of Scientific and Industrial Research (CSIR)-Central Leather Research Institute (CLRI), Chennai-600020, India

[∥]Department of Physics, Aliah University, Kolkata-700064, India

[⊥]Surface Physics Division, Saha Institute of Nuclear Physics, Kolkata-700064, India

[#]Academy of Scientific and Innovative Research (AcSIR), New Delhi-110001, India

Supporting Information

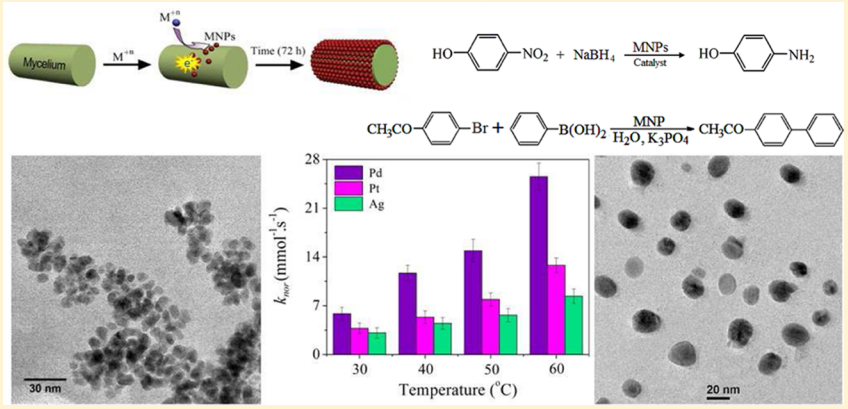

ABSTRACT: Increasing demand of noble-metal nanoparticles (MNPs) in catalysis research urges the development of a nontoxic, clean, and environmentally friendly methodology for the production of MNPs on solid surface. Herein we have developed a facile approach for biosynthesis of MNPs (Pd, Pt, and Ag) on the surface of *Rhizopous oryzae* mycelia through in situ reduction process without using any toxic chemicals. The size and shape of the biosynthesized MNPs varied among the MNPs, and "flower"-like branched nanoparticles were obtained in case of Pd and Pt, while Ag produced spheroidal nanoparticles. The cell-surface proteins of the mycelia acted as protecting, reducing, and shape-directing agent to control the size and shape of the synthesized MNPs. Proteins of 78, 62, and 55 kDa were bound on the MNPs surfaces and played a significant role in determining the morphology of the MNPs. The catalytic efficiency varied among the MNPs, and Pd nanoflower exhibited superior catalytic activities in both hydrogenation and Suzuki coupling reactions. Surface composition, concentration, and intracellular localization of MNPs determine the catalytic activity of the biosynthesized MNPs. The nanocatalyst could be easily separated and reused multiple times without significant loss in activity (95% average conversion). Overall, the understanding of this complex biomineralization mechanism and catalytic behavior at the nano−bio interface has provided an alternative for the synthesis of supported metal nanocatalyst to improve the environmental sustainability.

INTRODUCTION

In the ever expanding field of nanomaterial research, the catalytic application of noble-metal nanoparticles (MNPs) has attracted increasing attention in chemical reaction, energy conversion, fuel cells, pollution control, food processing, and so forth owing to their high surface area, increased accessibility to surface atoms, and lower coordination numbers compared with the bulk materials.[1−5] Recently, the shape-dependent properties of MNPs have stimulated their application in synthetic chemistry.[6−8] The hydrogenations and coupling are the most important chemical reactions for large scale production of pharmaceuticals, fine chemicals, polymers, plastics, and so on.[9,10] However, the majority of reactions are energy intensive, carried out in organic solvents, and give rise to environmental pollution. Besides, separation of the catalyst from the reaction medium and subsequent recycling remains a serious problem.

Received: August 13, 2014
Revised: September 26, 2014
Published: September 30, 2014

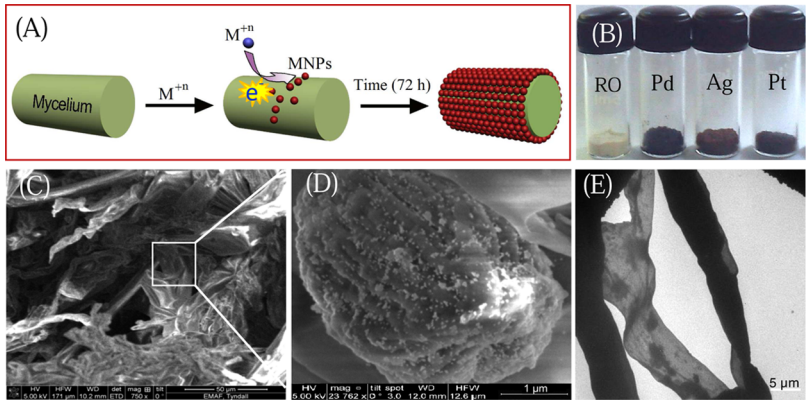

Figure 1. Schematic illustration (A) of the formation of MNPs (Pd, Pt, and Ag) on the mycelia surface. Color images (B) of *R. oryzae* (RO) and Pd, Pt, and Ag biomineralized mycelia. SEM micrograph at low (C) and high (D) magnifications of the *R. oryzae* mycelia after biomineralization of Pd. TEM micrograph (E) of *R. oryzae* mycelia after reaction with aqueous $PdCl_2$ solution.

In recent years much efforts have been devoted in designing and synthesis of water-based catalytic system utilizing easily separable and reusable heterogeneous catalyst. In this context, the supported MNPs with small size and uniform distribution offer a potential opportunity as recyclable heterogeneous catalyst.[11]

So far, several approaches have been introduced in recent years for the synthesis and fabrication of MNPs on various solid surfaces including metal oxide, polymers, resins, carbon nanotube, silica, and so on.[12−15] However, aggregation of the nanoparticles adversely affects the stability and catalytic efficiency. The surface of MNPs has been functionalized through post grafting method using different capping agents to overcome this limitation.[14] Unfortunately, most of the synthesis and functionalization procedures require frequent application of high temperature, pressure, highly inflammable organic solvents, and toxic chemicals, which often raise environmental and safety issues.[16−18] In addition, multistep preparation procedures often lead to inflated production cost. The control of uniform distribution of MNPs on the supportive material is also difficult, and use of capping agents occasionally impedes the catalytic behavior. Thus, the formation of MNPs on appropriate supportive material with tunable composition, shapes, and homogeneous distribution poses major challenge in the concerned area. The recent research strategy aims to develop a facile and cost-effective environmentally benign green technology for the synthesis of supportive MNPs as recyclable heterogeneous catalysts.[18]

The bioinspired or biomimetic approach provides a promising alternative in this direction and is emerging as a highly attractive green chemical methodology for the production of MNPs in aqueous solution.[19,20] In nature, several uni- and multicellular organisms reduce the metal ions as a detoxification mechanism and form nanomaterials.[20−30] Examples include the formation of calcium carbonate, siliceous materials, metal sulfides, iron oxide, gypsum, gold nanoparticles, and so on by *Bacillus stearothermophilus*, *Candida glabrata*, recombinant *Escherichia coli*, *Magnetospirillum magnetotacticum*, and *Rhizopus oryzae*, respectively. The cell wall of the microorganisms contains various functional groups, which promote the nucleation and organization of nanoparticles on the cell surface.[26,28] Although initial success has been achieved on biosynthesis of MNPs in the prokaryotic system, the formation of Pd, Pt, and Ag NPs on the surface of fungal mycelia has not been well understood. The fungal mycelia is more rigid and contains a large amount of functional groups compared with the bacteria; therefore, the mycelia surface is more appropriate for the formation of supportive MNPs.

Herein, we developed a facile bioinspired approach for the formation of Pd, Pt, and Ag NPs on the surface of *Rhizopus oryzae* and their catalytic applications as heterogeneous catalyst in organic solvent-free hydrogenation and Suzuki coupling reactions. To the best of our knowledge, this is the first report on in situ synthesis of "flower"-like branched Pd and PtNPs and spheroidal AgNPs through biosynthetic approach. To this end, the biomineralization mechanism of MNPs formation has been revealed through spectroscopic as well as proteomic analysis, and catalytic applications of the as-synthesized MNPs have been investigated in hydrogenation and Suzuki coupling reactions in aqueous solution. Results also demonstrated that the cell surface of *R. oryzae* prevented the aggregation of MNPs and leaching of metal ions from MNPs surface. The "flower"-like branched PdNPs exhibited superior catalytic activities in both hydrogenation and Suzuki coupling reactions. We strongly believe that our results will help to develop large-scale bioprocess of MNPs synthesis for advanced catalytic applications to improve environmental sustainability.

RESULTS AND DISCUSSION

Synthesis and Characterization of Bioinspired MNPs.

In situ "green chemical" synthesis of Pd, Pt, and Ag NPs on the surface of fungal mycelia has been described schematically in Figure 1A. In the current synthetic protocol the incubation of metal ions with *R. oryzae* mycelia leads to color change of the mycelia from pale white to light or dark brown (Figure 1B) depending on the formation of MNPs through electron transfer from mycelia surface to metal ions. The UV−vis spectroscopic measurements of the dispersed solution of biomineralized mycelia were recorded to characterize the MNPs. The spectrum (Supporting Information Figure S1) showed the appearance of a weak absorbance at ∼340 nm for PdNPs,[31] while Ag biomineralized mycelia demonstrated a surface plasmon resonance (SPR) band at 445 nm, AgNPs.[32] However, Pt-biomineralized mycelia did not exhibit any such absorption peak. The absorbance at ∼280 nm in both pristine and metal-ion-treated mycelia corresponds to the cell surface protein. In the treated mycelia, however, the absorbance was shifted ∼5 nm probably due to the interaction of surface protein with nanoparticles. In the in situ synthetic process, the reduction process was accomplished in aqueous solution without any

dx.doi.org/10.1021/jp508211t | J. Phys. Chem. C 2014, 118, 24623−24632

external reducing agent, therefore reducing the burden of toxic chemicals in the environment during nanoparticles synthesis process. The scanning electron microscope (SEM) image (Figure 1C) of Pd-biomineralized mycelia showed prominent change in surface morphology in comparison with the relatively smooth surface of the pristine mycelia (Supporting Information Figure S2). The high magnified image (Figure 1D) clearly revealed the formation of PdNPs on the mycelia surface. Similar images were also obtained in the case of AgNPs (data not shown); however, PtNPs were not detected on SEM images, which might be due to very small size. The representative transmission electron microscopic (TEM) image of Pd-biominaralized mycelia (Figure 1E) demonstrated densely coating of PdNPs on the mycelia surface. The synthetic process at different pH values (3.0−8.0) demonstrated that the formation of MNPs occurred through initial electrostatic binding of positively charged ionic species with negatively charged mycelia surface, followed by their reduction to MNPs on the mycelia surface (see Supporting Information for details).[26,28,33−35]

The yield of the biosynthesized nanoparticles was calculated based on accumulation of metals by the mycelia at optimum pH values (Supporting Information Figure S3). It was noted that ∼70−85% of metal ions were reduced to form MNPs depending on the metal ions. In particular, 80−85% of initial concentration of both silver and palladium were reduced to form nanoparticles in biomineralization process, whereas 71% reduction of platinum was observed. These indicated high conversion of metal ions to the corresponding MNPs in the proposed biomineralization process. Furthermore, the as-synthesized MNPs demonstrated high stability because the dispersed solution of MNPs did not show any shifting of SPR band during storage of the biomineralized mycelia for minimum 2 months at ambient temperature.

The size, shape, and crystallinity of the as-synthesized MNPs were determined from high-resolution transmission electron microscopy (HRTEM) images. The micrographs revealed that uniform distribution of nanoparticles throughout the surface, in addition to the variation in size and shape of the synthesized MNPs among the nanoparticles. Pd and Pt NPs exhibited "flower"-like branched nanostructures (Figure 2A,D) with average diameters of 25 and 3 nm, respectively. The high-magnified images (Figure 2B,E) showed that each nanostructure contains many small NPs, demonstrating that the "flower"-like branched nanostructures were formed by the selective binding of spherical NPs approaching from multiple directions to specific crystal faces of the initial small NPs.[7,27] The selected area electron diffraction (SAED) of Pd and Pt NPs showed the Scherrer ring patterns (inset of Figure 2B,E) associated with the [111], [200], [220], and [311] atomic planes and confirmed the formation of *fcc* crystal lattice of Pt and Pd NPs.[6] The formation of ∼19 nm spheroidal AgNPs (Figure 2G,H) was observed following treatment with $AgNO_3$ solution. The SAED pattern (Inset Figure 2H) was consistent with associated [111], [200], [222], and [311] planes of *fcc* nanocrystalline AgNPs.[32] The particle size distribution (PSD) histograms, measured from 150 nanoparticles in multiple TEM images, demonstrated that as-synthesized Pd, Pt, and AgNPs nanoparticles were highly monodisperse with average size of 24.5 ± 2.2, 3.3 ± 0.5, and 18.9 ± 2.5 nm, (Supporting Information Figure S4A−C), respectively. TEM images as well as PSD histogram data also revealed the high yield (70−80%) of desired shape of the biosynthesized MNPs. The biosynthesis of spherical MNPs has

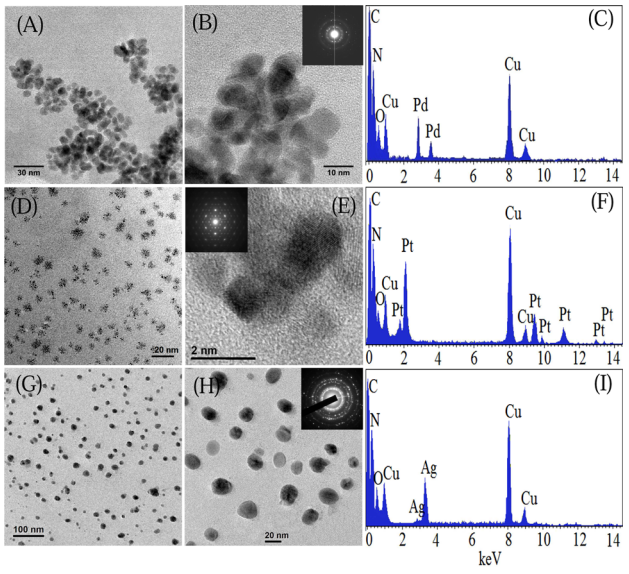

Figure 2. Low- and high-resolution TEM images of the synthesized Pd (A,B), Pt (D,E), and Ag (G,H) NPs after biomineralization process. SAED pattern (inset picture of B, E, and H) of the MNPs and EDXA spectra of the *R. oryzae* mycelia after biomineralization of Pd (C), Pt (F), and Ag (I).

been well reported in the literature; however, only very few studies demonstrated the formation of branched and non-spherical NPs.[36,37] To the best of our knowledge, this is the first report on the biosynthesis of branched Pd and Pt NPs and spheroidal AgNPs.

Area profile energy-dispersive X-ray (EDXA) analysis of the MNPs (Figure 2C,F,I) depicted the appearance of metal peaks (Pd, Pt, and Ag) along with C, N, and O peaks. The metal peaks correspond to the formation of MNPs, whereas C, N, K, and O arose from biomolecules present on the mycelia surface. Thus, the formation and conjugation of MNPs with mycelia surface occurred in a very close proximity, where mycelia acted as both reducing and template in the synthesis process. The concentrations of the synthesized nanoparticles on the mycelia surface were also quantitatively determined by EDXA measurement and were found to be 4.9, 3.1, and 5.8 wt %, respectively, of Pd, Pt, and AgNPs.

The crystalline nature of the biosynthesized Pt, Pd, and Ag NPs was confirmed by XRD analysis (Figure 3). The mycelia after PdNPs formation exhibited diffraction peaks at 39.5, 46.4, 67.2, 81, and 85.4°, which could be assigned to the (111), (200), (220), (331), and (222) planes, respectively, of face-

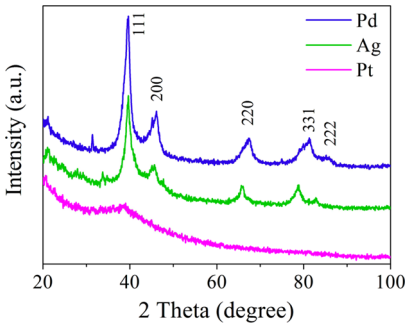

Figure 3. XRD pattern of the as-synthesized Pd, Pt, and Ag NPs on the mycelia surface after biomineralization process.

dx.doi.org/10.1021/jp508211t | J. Phys. Chem. C 2014, 118, 24623−24632

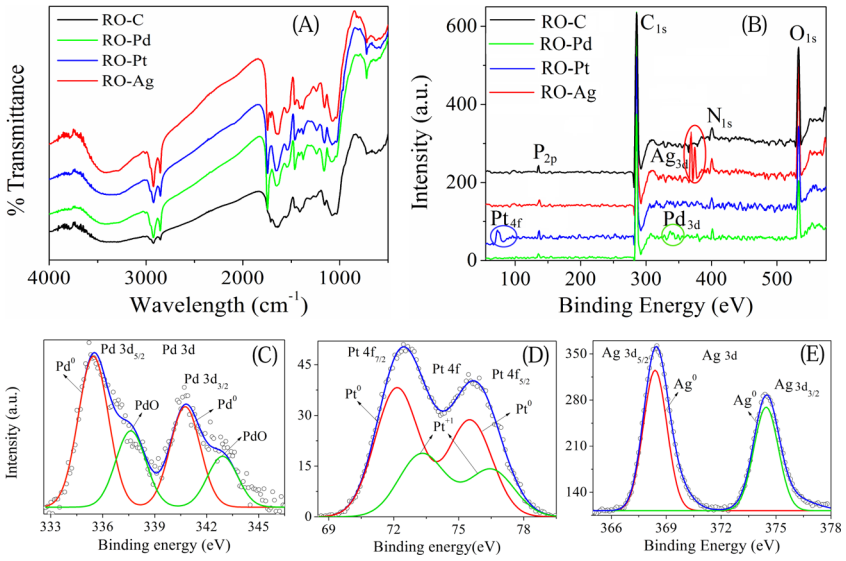

Figure 4. FTIR (A) and XPS survey (B) spectra of control and biomineralized mycelia after treatment with Pt, Pd, and Ag solution. Core-level XPS spectra of Pd 3d (C), Pt 4f (D), and Ag 3d (E) recorded on biomineralized mycelia.

centered cubic (fcc) metallic Pd crystal (JCPDS no. 46-1043). The XRD pattern of Pt-biomineralized sample had broadened, and the weak diffraction peak at $2\theta = 38.6°$ was assigned to the tiny PtNPs grown on the mycelia surface,[38] which is very consistent with the TEM result. Similarly, AgNP biomineralized samples showed a peak at 39° corresponding to the (111) plane of Ag nanocrystal. The (200), (220), (331), and (222) diffraction planes were located at 45.4, 65.5, 78.2, and 82.9° (JCPDS no. 00-004-0783), respectively. The results also showed that the main diffraction peaks of the as-synthesized MNPs are similar to pure MNPs and thus demonstrated that in situ fabrication of MNPs on mycelia surface did not produce any new crystal orientations of MNPs.

Biomineralization Mechanism of MNPs Formation. More insights into the formation mechanism and assembly of MNPs were carried out through X-ray photoelectron spectroscopy (XPS) and Fourier transform infrared (FTIR) analysis. The XPS spectra of the biomineralized mycelia showed core-level Pd 3d, Pt 4f, and Ag 3d peaks in addition to C 1s, N 1s, O 1s, and P 2p peaks, as shown in Figure 4B. The analysis of Pd 3d, Pt 4f, and Ag 3d spectra demonstrated the presence of different components of metals in the biomineralized mycelia.[39−41] The Pd 3d spectrum (Figure 4C) was composed of doublet peaks for $3d_{5/2}$ and $3d_{3/2}$ and appeared at 335.5 and 340.6 eV, respectively, which correspond to Pd^0.[39] In addition, high binding energy peaks of $3d_{5/2}$ and $3d_{3/2}$ for Pd^{2+} were also observed in the spectrum at 337.6 and 342.9 eV, respectively, indicating that part of the Pd^0 might be oxidized to PdO during the synthesis process. Similarly, two different chemical states of Pt $4f_{7/2}$ at 72.1 and 73.3 eV and Pt $4f_{5/2}$ at 75.5 and 76.5 eV were observed (Figure 4D) after treatment with platinum solution.[40] The low binding energy peaks originated from Pt^0 core, while the high binding energy peaks were attributed to the ionic form of metal ions (Pt^{1+}) bonded to the mycelia surface. However, in the silver-treated mycelia the spectrum (Figure 4E) showed Ag $3d_{5/2}$ and Ag $3d_{3/2}$ peaks at 368.3 and 374.4 eV, respectively, which correspond to the metallic species (AgNPs) only.[32]

In the pristine mycelia, the core-level C 1s, N 1s, O 1s, and P 2p spectra were resolved into different components of carboxyl, hydroxyl, amide, and phosphate groups of proteins (Supporting Information Figure S5), which provide metal ion binding sites for biomineralization process.[26,28,41] The clear shifting of core-level spectra of C 1s, N 1s, O 1s, and P 2p (Supporting Information Figure S6) were noted in the biomineralized mycelia in comparison with the control mycelia (see the Supporting Information for details). The carboxylate (O═C−OH), hydroxyl (C−OH), amide (HN−C═O), and acetal or hemiacetal (O−C−O) groups were shifted 0.4 to 0.7 eV binding energies due to binding of metal ions. Participation of phosphate bond in the biomineralization process was also demonstrated by shifting of P 2p spectrum in the higher binding energies. This clearly indicated that carboxyl, amine, and hydroxyl groups of the cell-surface proteins provided the metal ions binding sites and reduced them to MNPs through biomineralization process.

The FTIR spectrum (Figure 4A) of the pristine and biomineralized mycelia further confirmed the interaction of carboxyl, amine and hydroxyl groups of the cell surface proteins in the formation and stabilization of the MNPs. The FTIR spectrum of the pristine mycelia demonstrated the presence of carboxyl, hydroxyl, and amine groups due to strong IR signatures at 3415, 2927, 2851, 1715, 1644, 1547, 1464, 1409, 1302, 1237, and 1079 cm^{-1}.[27,42] Compared with the pristine mycelia, shifting of carboxyl, amine, and hydroxyl bands was noted after the formation of MNPs (see the Supporting Information). In the biomineralization process, the mycelia surface therefore sequestered the metal ions and or species through binding with carboxyl, amine, and hydroxyl groups of surface proteins and resulted in nucleation and growth of nanoparticles on the mycelia surface forming metal nanocomposite system. The surface protein of *R. oryzea* thus served as both reducing and stabilizing agents in the in situ green chemical synthesis of MNPs.

The specific role of surface protein in MNPs synthesis and biomineralization was studied through proteomic analysis. Initially, the surface protein(s) was extracted from the *R. oryzae* cell surface, and MNPs were synthesized by interaction of metal ions with the surface protein (see the Supporting Information). The metal solutions were turned light to deep

dx.doi.org/10.1021/jp508211t | J. Phys. Chem. C 2014, 118, 24623−24632

brown after 24 h of reaction (Figure 5A, inset) and exhibited SPR band (Figure 5A) corresponding to the MNPs. Protein

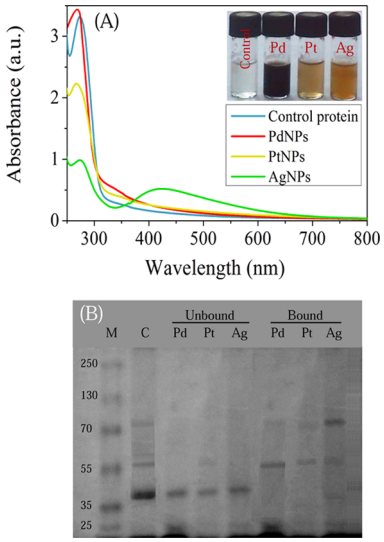

Figure 5. Color photograph (inset) and UV–vis spectra (A) of MNPs synthesized by *R. oryzae* surface protein. SDS-PAGE analysis (B) of *R. oryzae* surface protein responsible for synthesis of MNPs: control surface proteins (lane 2) and unbound proteins after synthesis of Pd (lane 3), Pt (lane 4), and Ag (lane 5) NPs and bound proteins released from Pd (lane 6), Pt (lane 7), and Ag (lane 8) NPs surface after boiling with 2% SDS solution.

concentration measurement further showed that proteins were bound on the nanoparticles surface (Supporting Information Table S1) during the in situ synthesis process and formed hard corona to stabilize the MNPs. The amount of bound and unbound proteins varied among the MNPs upon synthesis process. The bound and unbound proteins were also analyzed through SDS–PAGE. The electrophoresis pattern showed (Figure 5B) that protein bands of 78, 62, and 55 kDa molecular weight were absent in the unbound protein fraction compared with the control surface protein, suggesting that these proteins were likely to be bound on the MNPs surface and serving as capping agents in the synthesis process. Thus, bound proteins formed protein corona on the nanoparticles surfaces and controls the size, shape, and solubility of the biosynthesized MNPs. The bound proteins were released from the MNPs surface by boiling with 2% SDS solution and analyzed by SDS–PAGE to confirm this observation, which further showed the presence of 78, 62, and 55 kDa proteins in the bound fraction. The protein profile also illustrated clear differences in the protein corona composition among the MNPs, which is anticipated to the competitive and preferential binding of proteins to specific crystal faces of the nanoparticles.

In aqueous solution, the metal cations (Pd^{2+}, Pt^{2+}, and Ag^{+}) form hydrated species such as $[Pd(H_2O)_6]^{2+}$, $[Pt(OH)_2(aq)]$, $[Pt(H_2O)_4]^{2+}$, $[Ag(H_2O)_2]^{+}$, and other chloro/aqua complexes, respectively, at above pH 6.0.[33,43,44] The reduction potential of metal ions and their binding affinities to the proteins also varies among the metal ions (see the Supporting Information). The catalytic activity of the proteins and specific interaction of the adsorbed proteins on the nanoparticles surface therefore determine the shape control formation of MNPs. During nanoparticles synthesis process, the capping agent usually functions as the surface energy "modifier" to prevent aggregation of nanoparticles and control the shape of the nanoparticles as well.[45] The molecular interaction of the adsorbed proteins with nanoparticles surface controlled the crystallographic orientation of the nanoparticles and ultimately governed the shape of MNPs.[46−50] For instance, Pd-specific Pd4 peptide (TSNAVHPTLRHL) was used to synthesize spherical PdNPs[48] while self-assembling peptide-template (R5)-produced spherical, linear/ribbon-like, or network of PdNPs under varying concentration of Pd^{2+} ions.[49] Therefore, the most important factor is the intrinsic property of the surface proteins of *R. oryzae*, which regulate the size- and shape-controlled formation of biosynthesized MNPs.

Catalytic Hydrogenation and Suzuki Coupling Reaction. The catalytic activities of the metal nanocomposites were then studied for aqueous phase hydrogenation and Suzuki coupling reactions. The catalytic hydrogenation activity (Supporting Information Figure S7A) of nanocomposites was quantitatively evaluated in the reduction of *p*-nitrophenol (*p*-NP) to *p*-aminophenol (*p*-AP) by sodium borohydride ($NaBH_4$). Upon the addition of nanocomposite to the reaction medium containing aqueous solution of *p*-NP and $NaBH_4$, the absorption intensity at 400 nm decreased successively with time, accompanied by simultaneous appearance of a new peak at 300 nm corresponding to *p*-AP.[6,7] The reaction was completed within 5 to 25 min depending on the MNPs in the nanocomposite (Supporting Information Table S2) and confirmed by color change from bright-yellow solution (*p*-NP) to colorless *p*-AP. The control experiment, without the addition of nanocomposite, remained bright yellow and did not show any change of absorbance at 400 nm with time, indicating that the reduction of *p*-NP to *p*-AP was catalyzed by metal nanocomposites. Figure 6A shows the time-dependent absorption spectra of *p*-NP reduction by the nanocomposite at 30 ± 2 °C. For all nanocomposites, upon the addition of the catalyst in reaction medium, a certain time was required prior to initiate the hydrogenation reaction. This time is referred to as an induction time t_{ind} and required for adsorption of *p*-NP on the catalyst's surface before initiation of the reaction. Diffusion of *p*-NP through the mycelia surface to interact with the internally localized MNPs may also responsible for t_{ind}. Among all nanocomposites, PdNPs had the lowest t_{ind}, as shown in Figure 6B. The t_{ind} was found to decrease with increasing temperature (Supporting Information Table S2), suggesting that at higher temperature perhaps more *p*-NP were diffused through the mycelia and adsorbed on the catalyst surface, which favored the hydrogenation reaction.

The hydrogenation reaction followed pseudo-first-order rate kinetics, and the apparent rate constant (k_{app}) was determined from the slope of linear regression of ln *A* (*A* = absorbance at 400 nm) versus time after t_{ads}.[7] The average k_{app} calculated at different temperatures was found to increase with increasing temperature (Supporting Information Table S2) and followed the order as PdNPs > AgNPs > PtNPs. To compare the catalytic efficiency of the nanocomposites, we measured k_{nor} (normalized rate constant) values at different temperature (Figure 6C) by dividing k_{app} values with the amounts of Pd, Pt, and Ag present in the nanocomposite. It was noted that the k_{nor} values followed the order as PdNPs > PtNPs > AgNPs, and activities of all nanocomposites were higher or comparable to those of chemically synthesized MNPs (Supporting Information Table S3).[51−54]

dx.doi.org/10.1021/jp508211t | J. Phys. Chem. C 2014, 118, 24623−24632

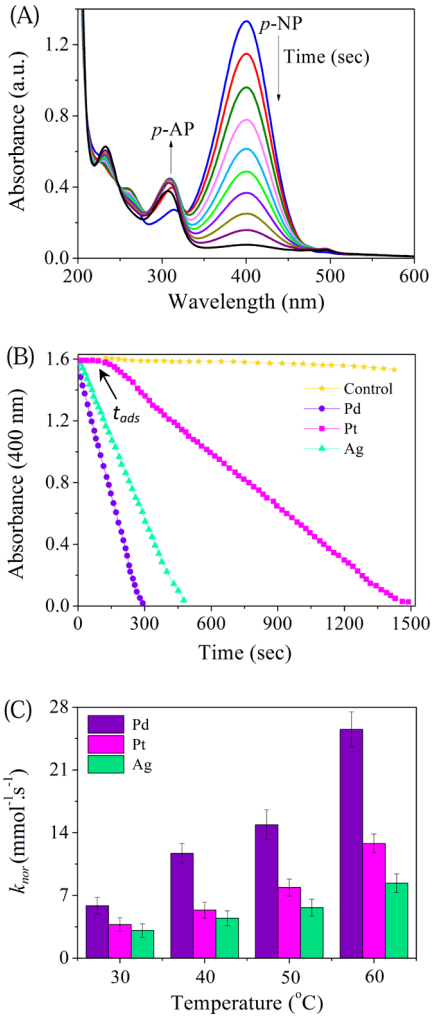

Figure 6. Time-dependent absorption spectra (A) of the reaction solution in the presence of metal nanocomposites as a catalyst. Normalized absorbance (B) at the peak position of *p*-NP (400 nm) as a function of time and plot (C) of normalized rate constant (k_{nor}) against temperature.

The activation energy (E_a) is an important parameter for all chemical reactions including catalysis and was determined from the Arrhenius equation (eq 1)

$$\ln k_{nor} = \ln A - E_a/RT \quad (1)$$

where k_{nor}, A, and R are normalized rate constant of the reaction at temperature T (in Kelvin), prefactor, and universal gas constant, respectively. The activation energy (E_a) of the hydrogenation reaction was measured from the slope ($-E_a/R$) of linear regression of ln k_{nor} against $1/T$ and varied in the range of 26.59 ± 5.3 to 38.41 ± 2.4 kJ mol^{-1} (Supporting Information Table S2) depending on the MNPs. It interesting to note that among all MNPs, Pd nanocomposite exhibited the highest catalytic activity, although it has higher activation energy. Similarly, Ag nanocomposite demonstrated the lowest catalytic activity with lowest activation energy. Therefore, we are confident to propose that besides surface composition other factors also influenced the catalytic activity.

The coupling reaction is another important metal-catalyzed C−C bond formation reaction for the production of industrially important chemicals; however, most of the reactions are carrying out in highly flammable organic solvents. Therefore, the aqueous phase-coupling reaction has wide industrial applications for the development of sustainable chemistry. In this context, the Suzuki coupling reaction in the C−C bond formation (Supporting Information Figure S7B) of phenylboronic acid and *p*-bromoacetophenone in aqueous solution was studied using the as-synthesized Pd, Pt, and Ag nanocomposites. A complete conversion (>99%) was achieved using Pd nanocomposite (Supporting Information Figure S8) within 5 h, but Pt and Ag nanocomposites were unable to initiate the reaction in aqueous medium. Very poor activity of Pt and Ag NPs in Suzuki coupling reaction is also reported in the literature.[55,56] The PdNPs were reused multiple times in coupling reaction (see Recyclability of MNPs section), and overall 95% conversion yield was obtained. The average yield of the PdNP-catalyzed coupling reaction was further compared with chemically synthesized MNPs. There are several articles on synthesis of PdNPs using micelles, microemulsions, surfactants, different ligands, mesoporous materials, zeolites, ionic liquids, and so on; however, we delighted to note that the overall yield of the Suzuki coupling by as-synthesized PdNPs is higher or very comparable to those of the chemically synthesized MNPs (Supporting Information Table S4).[56−58] It is also interesting to observe that most of the coupling reactions in the literatures are reported to be carried out with iodo substrate and in organic solvents;[56−58] however, in the present study, 95% (average) conversion was achieved using the biosynthesized Pd nanoflower in aqueous solution with bromo substrate, which is usually difficult to achieve with less active bromo substrate.

The catalytic reaction of MNPs is proposed to be exhibited by MNP itself or by metal ions leached out from the nanoparticles.[56,57] It is important to note that biosynthesized MNPs were washed thoroughly with double-distilled water to remove any unbound or loosely bound metal ions from the nanoparticles surface. In addition, the leaching of metal ions in the solution was not detected during course of the catalysis reaction, suggesting MNP-mediated catalytic reaction. To further understand the catalytic reaction, we recorded TEM images of the thin section of biomineralized mycelia, which showed the formation of MNPs on the cell surface, periplasmic space, and cytosolic region of the mycelia (Supporting Information Figure S9). On the basis of the composition and morphology of the synthesized MNPs, the MNP synthesized on the cell surface as well as in the intracellular region may take part in the catalytic reaction. The observed induction time t_{ind} in Figure 6B suggest that *p*-NP might diffuse through mycelia to interact with the intracellularly localized MNPs. The reactants could penetrate the surface of the mycelia and interacted with the intracellularly localized MNPs to generate products, which then diffused out into aqueous medium. In addition, the higher activation energy of Pd nanocomposite (Supporting Information Table S2) suggests that the size and shape of the MNPs control not only the catalytic activity but also other factors like diffusion of the reactants through the mycelia, concentration, and position of the MNPs in the intracellular region of the mycelia, which may have crucial role in the catalytic activity. El-Sayed et al.[56,58] reported that (100) and (111) facets of PdNPs played the major role in Suzuki coupling reactions, whereas Knecht et al.[49] demonstrated that size and shape of the MNPs as well as the diffusion of the reactants through the peptide templates including the position of the nanoparticles within the peptide template alter the catalytic activity. Very recently, we also demonstrated that the

dx.doi.org/10.1021/jp508211t | J. Phys. Chem. C 2014, 118, 24623−24632

catalytic activity of protein-conjugated AuNPs in *p*-NP reduction is sensitive to both size of the nanoparticles and thickness of the protein corona.[7] The HRTEM images (Figure 2B,E) revealed that "flower"-shaped Pd and Pt nanostructure composed of several small nanoparticles caused exposure of catalytically active certain high-index facets,[6] which favor the catalytic reactions. It is also interesting to note that Pd nanocomposite has negligible t_{ind} value, while Pt nanocomposite has the highest t_{ind} value in the series (Figure 6B). Therefore, in the present catalytic reactions, the differential catalytic activity of the biosynthesized MNPs is anticipated to be likely due to the cumulative effects of the morphology, concentration, and intracellular localization of MNPs in the mycelia. The size and shape of the MNPs determine the degree of interaction between the reactants and MNPs, while the intracellular localization and concentration of the MNPs modulate diffusion of the reactants and ultimately govern the catalytic behavior. Therefore, the catalytic activity of the biosynthesized MNPs can be tuned at the synthetic level. However, detailed analysis of contribution of cell surface and intracellularly localized MNPs in catalytic reaction is the subject of ongoing work.

Recyclability of MNPs. The separation and reuse of the catalysts in successive reactions is another important aspect for making the chemical process cost-effective and prevent their accumulation in waste. The recyclability of the catalyst was tested following their separation from the reaction mixture. The MNPs were easily separated from the reaction medium by centrifugation. The recovered catalysts were washed with dichloromethane, dried, and finally used for multiple cycles of hydrogenation and coupling reaction under identical reaction conditions. Results (Supporting Information Table S5) showed that the conversion yield of *p*-NP was still as high as 99.5% in the second cycle of the reaction and did not exhibit significant loss of catalytic activity in multiple reuses; the yield was still above 95% in the fifth cycles of the reaction.

Similarly, in the coupling reaction 96% conversion was achieved in the second cycle and dropped to 90% in fifth cycle of the reaction. Therefore, the overall conversion was calculated to be 95%, which demonstrated good catalytic activity and good recycling potential[57,59] of the biosynthesized MNPs. This is in contrast with the results of El-Sayed et al.,[58] who reported ∼15% drop in Suzuki coupling reaction by PVP-Pd nanoparticles in the second cycle only even with more active iodo substrate. Choi et al.[60] also reported that 98.9% yield was obtained in the first cycle of the Suzuki reaction by Pd−Ag/ZnO; however, in the fifth cycle of the reaction, 81.5% yield was obtained.

The loss of catalytic activity in the successive cycles generally occurs due to aggregation or precipitation of MNPs in the reaction medium and leaching of metal ions.[56,57] The precipitation and leaching metal ions were measured by atomic absorption spectroscopy (see Experimental Section) to understand the stability of the nanoparticles and mechanism of catalysis reaction. However, during the course of the catalytic reaction we did not notice either precipitation of MNPs in the reaction medium or leaching of metal ions from MNPs, which confirm the high stability of the biosynthesized metal nanocomposite. The microbial cell surface sufficiently stabilizes the MNPs by preventing their aggregation, precipitation, and leaching of metal ions, thus producing a good catalyst with high efficiency and stability. The high catalytic efficiency, stability, and recyclability of the metal nanocomposite will therefore lead to the development of microbial synthesis of stable green catalytic nanoreactors.

■ CONCLUSIONS

In conclusion, we have developed a facile biosynthetic route for environmental benign cost-effective productions of various MNPs (Pd, Pt, and Ag) on the surface of fungal mycelia. The MNPs were synthesized through an electrostatic interaction of metal ions, followed by their reduction to nanoparticles by surface proteins. The MNPs were homogeneously distributed throughout the surface, and their size and shape varied depending on the MNPs. The "flower"-like branched nanoparticles were obtained in the case of Pd and Pt, while Ag produced spheroidal nanoparticles. Protein profile analysis confirmed that cell surface protein played a significant role in determining the size and shape of the MNPs. The as-prepared MNPs exhibited high catalytic activities in hydrogenation and Suzuki coupling reactions in aqueous solution. The catalytic efficiency varied with the type of MNPs, and the high index branched Pd nanoflower exhibited superior catalytic activity (>99% conversion) in both chemical reactions. Moreover, the nanocatalyst can be easily separated and reused multiple times without significant loss in activity (95% average conversion). Overall, this biosynthetic approach has provided an alternative for environmental benign synthesis of supported nanoparticles as heterogeneous catalyst, which will find potential application in many industrially important catalytic processes.

■ EXPERIMENTAL SECTION

Synthesis of MNPs on Fungal Surface. Biosynthesis of MNPs in aqueous medium was carried out through the reduction of metal ions solution (Pd^{2+}, Pt^{2+}, and Ag^{+}) by *R. oryzae* (see Supporting Information). In typical experiments, blotted dried fungal mycelia (0.25 g) were added separately to 25 mL of aqueous solution of different metal ions (2.0−5.0 mM) and incubated at 60 °C for 72 h under shaking (150 rpm) condition in the absence of any external reducing agent. The bioreduction of metal ions was monitored by UV−vis spectroscopy (Varian Cary 100 Bio, USA) measurement of the dispersed solution of mycelia as well as color change of the mycelia. The control experiments were also carried out under identical conditions without the addition of fungal mycelia. The effect of pH on nanoparticle synthesis was studied by varying pH of the metal ions solution from 3.0−8.0, keeping other conditions remain same. The pH of the metal solution was adjusted by direct addition of 1 M HCl or 1 M NaOH to the metal solution to get the desired pH value. The experiments were not conducted at pH >8.0 to avoid microprecipitations of metal as hydroxide.

Estimation of Metal Ions Concentration. The concentrations of metal ions before and after interaction with *R. oryzae* were determined by flame atomic absorption spectrometer (AAS, Nova 350, Analytic Jena, Germany) with respective standard solution, and the amount of metal uptake by the mycelia was calculated using mass-balance equation.[35]

Characterization of Metal Nanoparticles. The size, shape, crystallinity, and elemental analysis of the as-synthesized MNPs were analyzed by HRTEM (JEOL JEM 2010, Japan) operated at an accelerating voltage of 200 kV. The size distribution of MNPs was measured from multiple HRTEM images. The elemental analysis of the samples was carried out in EDXA system attached with HRTEM instrument. The

dx.doi.org/10.1021/jp508211t | J. Phys. Chem. C 2014, 118, 24623−24632

amount of metal (weight percentage) present in the nanocomposites was calculated by EDXA. The crystal structures were analyzed from SAED patterns recorded from HRTEM images. Powder X-ray diffraction (XRD) analysis was carried out on a Philips XRD with Cu Kα radiation (λ = 1.54 Å). The biomineralization mechanism was studied by FTIR and XPS measurements of the pristine and metal-ion-treated mycelia using Shimadzu FTIR and Omicron Multiprobe (Omicron NanoTechnology, U.K.) spectrometer, respectively.

Proteomic Analysis. After synthesis of MNP by surface protein (see Supporting Information for details), the unbound proteins were isolated and separated by SDS-PAGE. The concentration of bound and unbound proteins was measured by Bradford method.[61] The bound proteins were released from MNPs surface by boiling with sample loading buffer containing 2% SDS for 10 min and further analyzed by SDS−PAGE.

Catalytic Activity of MNPs. The catalytic hydrogenation reaction of metal nanocomposites was studied using borohydride reduction of *p*-NP as a model system. In a typical experiment, 0.1 mL of aqueous *p*-NP solution (3 mM) was added to 2.8 mL of double-distilled water containing 2 ± 0.2 mg of nanocomposite. To this solution, a freshly prepared 0.1 mL of sodium borohydride ($NaBH_4$) solution (0.3 M) was added. The control experiment was carried out under identical conditions except the addition of nanocomposite. The conversion of *p*-NP to *p*-AP was then monitored spectrophotometrically.

The solvent-free Suzuki coupling reaction of phenylboronic acid and *p*-bromoacetophenone was studied with the bioinspired synthesized metal nanocomposites as a model reaction. The reaction was carried out in aqueous medium instead of organic solvent. In brief, phenylboronic acid (365.8 mg, 3 mmol) and *p*-bromoacetophenone (398 mg, 2 mmol) were dissolved in 3 mL of double-distilled water. Potassium carbonate (552.8 mg, 4 mmol) was then added to this solution. The reaction mixture was purged with nitrogen gas, followed by the addition of 15 ± 0.5 mg of metal nanocomposites to initiate the reaction. The solution was stirred for 5 h under refluxing condition, and the reaction product was analyzed by TLC and ^{1}H NMR. The concentration of Pd, Pt, and Ag in the nanocomposites was 4.9, 3.1, and 5.8 wt % age, respectively, in both catalytic reactions.

Recyclability of MNPs. The recyclability of the catalyst was tested to minimize the accumulation of the catalyst in waste and to reduce the production cost of nanoparticles synthesis as well as catalysis reaction. After catalysis reaction, MNPs were recovered from the reaction mixture by centrifugation (10 000 rpm, 10 min), washed with dichloromethane, and dried. The dried catalysts were used in successive cycle adopting similar procedure as previously described.

Precipitation and Leaching of Metal Ions from MNPs. The precipitation and leaching of metal ions from MNPs were tested to understand the mechanism of catalysis reaction and stability of the MNPs. The concentration of metal ions in the solution after catalysis reaction was measured using AAS analysis with appropriate standard metal solution.

■ ASSOCIATED CONTENT

Supporting Information

Other experimental details and additional results. This material is available free of charge via the Internet at http://pubs.acs.org.

■ AUTHOR INFORMATION

Corresponding Authors

*S.K.D.: E-mail: sujoy@clri.res.in; sujoydasiacs@gmail.com. Tel: +914424437133. Fax: +914424911589.

*A.B.M.: E-mail: abmandal@hotmail.com. Tel: +914424910846. Fax: +914424912150.

Notes

The authors declare no competing financial interest.

■ ACKNOWLEDGMENTS

S.K.D. acknowledges Department of Science and Technology (DST), Government of India for research support under Fast Track Research Scheme (SR/FT/LS-80/2012) and Department of Biotechnology (DBT), Government of India under RGYI Scheme (BT/PR6433/GBD/27/413/2012). We also thank Dr. Debasis Samanta, Polymer Division, CSIR−CLRI (CSIR-CLRI communication number 1020) for valuable suggestions.

■ REFERENCES

(1) Yao, Y.; Xue, M.; Zhang, Z.; Zhang, M.; Wang, Y.; Huang, F. Gold Nanoparticles Stabilized by an Amphiphilic Pillar[5]arene: Preparation, Self-assembly Into Composite Microtubes in Water and Application in Green Catalysis. *Chem. Sci.* **2013**, *4*, 3667−3672.

(2) Shao, L.; Zhang, B.; Zhang, W.; Hong, S. Y.; Schlögl, R.; Su, D. S. The Role of Palladium Dynamics in the Surface Catalysis of Coupling Reactions. *Angew. Chem., Int. Ed.* **2013**, *52*, 2114−2117.

(3) Das, S. K.; Khan, M. M. R.; Guha, A. K.; Das, A. R.; Mandal, A. B. Silver-nano Biohybride Material: Synthesis, Characterization and Application in Water Purification. *Bioresour. Technol.* **2012**, *124*, 495−499.

(4) Zhang, P.; Li, R.; Huang, Y.; Chen, Q. A Novel Approach for the in Situ Synthesis of Pt−Pd Nanoalloys Supported on Fe_3O_4@C Core−Shell Nanoparticles with Enhanced Catalytic Activity for Reduction Reactions. *ACS Appl. Mater. Interfaces* **2014**, *6*, 2671−2678.

(5) Nadagouda, M. N.; Varma, R. S. Synthesis of Thermally Stable Carboxymethyl Cellulose/Metal Biodegradable Nanocomposites for Potential Biological Applications. *Biomacromolecules* **2007**, *8*, 2762−2767.

(6) Mohanty, A.; Garg, N.; Jin, R. A Universal Approach to the Synthesis of Noble Metal Nanodendrites and Their Catalytic Properties. *Angew. Chem., Int. Ed.* **2010**, *49*, 4962−4966.

(7) Das, S. K.; Dickinson, C.; Lafir, F.; Brougham, D. F.; Marsili, E. Synthesis, Characterization and Catalytic Activity of Gold Nanoparticles Biosynthesized with *Rhizopus oryzae* Protein Extract. *Green Chem.* **2012**, *14*, 1322−1334.

(8) Zeng, J.; Zhang, Q.; Chen, J.; Xia, Y. A Comparison Study of the Catalytic Properties of Au-Based Nanocages, Nanoboxes, and Nanoparticles. *Nano Lett.* **2010**, *10*, 30−35.

(9) Mitsudomea, T.; Kaneda, K. Gold Nanoparticle Catalysts for Selective Hydrogenations. *Green Chem.* **2013**, *15*, 2636−2654.

(10) Dong, F.; Guo, W.; Park, S.-K.; Ha, C.-S. Controlled Synthesis of Novel Cyanopropyl Polysilsesquioxane Hollow Spheres Loaded with Highly Dispersed Au Nanoparticles for Catalytic Applications. *Chem. Commun.* **2012**, *48*, 1108−1110.

(11) Dhakshinamoorthy, A.; Garcia, H. Catalysis by Metal Nanoparticles Embedded on Metal−Organic Frameworks. *Chem. Soc. Rev.* **2012**, *41*, 5262−5284.

(12) Dutta, S.; Ray, C.; Sarkar, S.; Pradhan, M.; Negishi, Y.; Pal, T. Silver Nanoparticle Decorated Reduced Graphene Oxide (rGO) Nanosheet: A Platform for SERS Based Low-Level Detection of Uranyl Ion. *ACS Appl. Mater. Interfaces* **2013**, *5*, 8724−8732.

(13) White, R. J.; Luque, R.; Budarin, V. L.; Clark, J. H.; Macquarrie, D. J. Supported Metal Nanoparticles on Porous Materials. Methods and Applications. *Chem. Soc. Rev.* **2009**, *38*, 481−494.

(14) Shen, C.; Wang, Y. J.; Xu, J. H.; Wang, K.; Luo, G. S. Size Control and Catalytic Activity of Highly Dispersed Pd Nanoparticles Supported on Porous Glass Beads. *Langmuir* **2012**, *28*, 7519−7527.
(15) Liu, J.; Yang, H. Q.; Kleitz, F.; Chen, Z. G.; Yang, T.; Strounina, E.; Lu, G. Q.; Qiao, S. Z. Yolk−Shell Hybrid Materials with a Periodic Mesoporous Organosilica Shell: Ideal Nanoreactors for Selective Alcohol Oxidation. *Adv. Funct. Mater.* **2012**, *22*, 591−599.
(16) Dahl, J. A.; Maddux, B. L. S.; Hutchison, J. E. Toward Greener Nanosynthesis. *Chem. Rev.* **2007**, *107*, 2228−2269.
(17) Nadagouda, M. N.; Varma, R. S. Green Synthesis of Silver and Palladium Nanoparticles at Room Temperature Using Coffee and Tea Extract. *Green Chem.* **2008**, *10*, 859−862.
(18) Das, S. K.; Khan, M. M. R.; Guha, A. K.; Naskar, N. Bio-inspired Fabrication of Silver Nanoparticles on Nanostructured Silica: Characterization and Application as a Highly Efficient Hydrogenation Catalyst. *Green Chem.* **2010**, *15*, 2548−2557.
(19) Cölfen, H. Biomineralization: A Crystal-Clear View. *Nat. Mater.* **2010**, *9*, 960−961.
(20) Mann, S. Molecular Tectonics in Biomineralization and Biomimetic Materials Chemistry. *Nature* **1993**, *365*, 499−505.
(21) Park, T. J.; Lee, S. Y.; Heo, N. S.; Seo, T. S. *In vivo* Synthesis of Diverse Metal Nanoparticles by Recombinant *Escherichia coli*. *Angew. Chem., Int. Ed.* **2010**, *49*, 7019−7024.
(22) Shenton, W.; Pum, D.; Sleytr, U. B.; Mann, S. Synthesis of Cadmium Sulphide Superlattices using Self-assembled Bacterial S-layers. *Nature* **1997**, *389*, 585−587.
(23) Lee, Y.; Kim, J.; Yun, D. S.; Nam, Y. S.; Horn, Y. S.; Belcher, A. M. Virus-Templated Au and Au−Pt Core−Shell Nanowires and Their Electrocatalytic Activities for Fuel Cell Applications. *Energy Environ. Sci.* **2012**, *5*, 8328−8334.
(24) Du, L.; Xian, L.; Feng, J.-X. Rapid Extra-/Intracellular Biosynthesis of Gold Nanoparticles by the Fungus *Penicillium* sp. *J. Nanopart. Res.* **2011**, *13*, 921−930.
(25) Ramanathan, R.; Field, M. R.; O'Mullane, A. P.; Smooker, P. M.; Bhargava, S. K.; Bansal, V. Aqueous Phase Synthesis of Copper Nanoparticles: A Link Between Heavy Metal Resistance and Nanoparticle Synthesis Ability in Bacterial Systems. *Nanoscale* **2013**, *5*, 2300−2306.
(26) Das, S. K.; Liang, J.; Schmidt, M.; Laffir, F.; Marsili, E. Biomineralization Mechanism of Gold by Zygomycete Fungi *Rhizopous oryzae*. *ACS Nano* **2012**, *6*, 6165−6173.
(27) Das, S. K.; Das, A. R.; Guha, A. K. Microbial Synthesis of Multishaped Gold Nanostructures. *Small* **2010**, *6*, 1012−1021.
(28) Das, S. K.; Das, A. R.; Guha, A. K. Gold Nanoparticles: Microbial Synthesis and Application in Water Hygiene Management. *Langmuir* **2009**, *25*, 8192−8199.
(29) Reith, F.; Etschmann, B.; Grosse, C.; Moors, H.; Benotmane, M. A.; Monsieurs, P.; Grass, G.; Doonan, C.; Vogt, S.; Lai, B.; et al. Mechanisms of Gold Biomineralization in the Bacterium *Cupriavidus metallidurans*. *Proc. Natl. Acad. Sci. U.S.A.* **2009**, *106*, 17757−17762.
(30) Narayanan, K. B.; Sakthivel, N. Biological Synthesis of Metal Nanoparticles by Microbes. *Adv. Colloid Interface Sci.* **2010**, *156*, 1−13.
(31) Li, Y.; Hong, X. M.; Collard, D. M.; El-Sayed, M. A. Suzuki Cross-Coupling Reactions Catalyzed by Palladium Nanoparticles in Aqueous Solution. *Org. Lett.* **2000**, *2*, 2385−2388.
(32) Das, S. K.; Khan, M. M. R.; Paranthamon, T.; Laffir, F.; Guha, A. K.; Sekaran, G.; Mandal, A. B. Nano-silica Fabricated with Silver Nanoparticles: Antifouling Adsorbent for Efficient Dye Removal, Effective Water Disinfection and Biofouling Control. *Nanoscale* **2013**, *5*, 5549−5560.
(33) Azaroual, M.; Romand, B.; Freyssinet, P.; Disnar, J.-R. Solubility of Platinum in Aqueous Solutions at 25 °C and pHs 4 to 10 Under Oxidizing Conditions. *Geochim. Cosmochim. Acta* **2001**, *65*, 4453−4466.
(34) Das, S. K.; Shome, I.; Guha, A. K. Surface Functionalization of *Aspergillus versicolor* Mycelia: I*n situ* Fabrication of Cadmium Sulphide Nanoparticles and Removal of Cadmium Ions from Aqueous Solution. *RSC Adv.* **2012**, *2*, 3000−3007.
(35) Das, S. K.; Bhowal, J.; Das, A. R.; Guha, A. K. Adsorption Behavior of Rhodamine B on *Rhizopus oryzae* Biomass. *Langmuir* **2006**, *22*, 7265−7272.
(36) Mahmoud, A.; Tabor, C. E.; El-Sayed, M. A.; Ding, Y.; Wang, Z. L. A New Catalytically Active Colloidal Platinum Nanocatalyst: The Multiarmed Nanostar Single Crystal. *J. Am. Chem. Soc.* **2008**, *130*, 4590−4591.
(37) Lim, B.; Jiang, M.; Camargo, P. H. C.; Cho, E. C.; Tao, J.; Lu, X.; Zhu, Y.; Xia, Y. Pd-Pt Bimetallic Nanodendrites with High Activity for Oxygen Reduction. *Science* **2009**, *324*, 1302−1305.
(38) Jin, Z.; Xiao, M.; Bao, Z.; Wang, P.; Wang, J. A General Approach to Mesoporous Metal Oxide Microspheres Loaded with Noble Metal Nanoparticles. *Angew. Chem., Int. Ed.* **2012**, *51*, 6406−6410.
(39) Lim, J.-S.; Kim, S.-M.; Lee, S.-Y.; Stach, E. A.; Culver, J. N.; Harris, M. T. Biotemplated Aqueous-Phase Palladium Crystallization in the Absence of External Reducing Agents. *Nano Lett.* **2010**, *10*, 3863−3867.
(40) Tseng, R. J.; Tsai, C.; Ma, L.; Ouyang, J.; Ozkan, C. S.; Yang, Y. Digital Memory Device Based on Tobacco Mosaic Virus Conjugated with Nanoparticles. *Nat. Nanotechnol.* **2006**, *1*, 72−77.
(41) Das, S. K.; Mukherjee, M.; Guha, A. K. Interaction of Chromium with Resistant Strain *Aspergillus versicolor*: Investigation with Atomic Force Microscopy and Other Physical Studies. *Langmuir* **2008**, *24*, 8643−8650.
(42) Silverstein, R. M.; Bassler, G. C.; Morrill, T. C. *Spectrometric Identification of Organic Compounds*, 4th ed.; Wiley: New York, 1981.
(43) Avery, K. N.; Schaak, J. E.; Schaak, R. E. M13 Bacteriophage as a Biological Scaffold for Magnetically-Recoverable Metal Nanowire Catalysts: Combining Specific and Nonspecific Interactions To Design Multifunctional Nanocomposites. *Chem. Mater.* **2009**, *21*, 2176−2178.
(44) Cotton, F. A.; Wilkinson, G. *Advanced Inorganic Chemistry*, 5th ed.; Wiley: New York, 1988.
(45) Tao, A. R.; Habas, S.; Yang, P. Shape Control of Colloidal Metal Nanocrystals. *Small* **2008**, *4*, 310−325.
(46) Sewell, S. L.; Wright, D. W. Biomimetic Synthesis of Titanium Dioxide Utilizing the R5 Peptide Derived from *Cylindrotheca fusiformis*. *Chem. Mater.* **2006**, *18*, 3108−3113.
(47) Cole, K. E.; Ortiz, A. N.; Schoonen, M. A.; Valentine, A. M. Peptide- and Long-Chain Polyamine- Induced Synthesis of Micro- and Nanostructured Titanium Phosphate and Protein Encapsulation. *Chem. Mater.* **2006**, *18*, 4592−4599.
(48) Pandey, R. B.; Heinz, H.; Feng, J.; Farmer, B. L.; Slocik, J. M.; Drummy, L. F.; Naik, R. R. Adsorption of Peptides (A3, Flg, Pd2, Pd4) on Gold and Palladium Surfaces by a Coarse-grained Monte Carlo Simulation. *Phys. Chem. Chem. Phys.* **2009**, *11*, 1989−2001.
(49) Jakhmola, A.; Bhandari, R.; Pacardo, D. B.; Knecht, M. R. Peptide Template Effects for the Synthesis and Catalytic Application of Pd Nanoparticle Networks. *J. Mater. Chem.* **2010**, *20*, 1522−1531.
(50) Coppage, R.; Slocik, J. M.; Briggs, B. D.; Frenkel, A. I.; Naik, R. R.; Knecht, M. R. Determining Peptide Sequence Effects That Control the Size, Structure, and Function of Nanoparticles. *ACS Nano* **2012**, *6*, 1625−1636.
(51) Rashid, M. H.; Mandal, T. K. Templateless Synthesis of Polygonal Gold Nanoparticles: An Unsupported and Reusable Catalyst with Superior Activity. *Adv. Funct. Mater.* **2008**, *18*, 2261−2271.
(52) Kumar, S. S.; Kumar, C. S.; Mathiyarasu, J.; Phani, K. L. Stabilized Gold Nanoparticles by Reduction Using 3,4-Ethylenedioxythiophene-polystyrenesulfonate in Aqueous Solutions: Nanocomposite Formation, Stability, and Application in Catalysis. *Langmuir* **2007**, *23*, 3401−3408.
(53) Rashid, M. H.; Raula, M.; Mandal, T. K. Polymer Assisted Synthesis of Chain-like Cobalt-Nickel Alloy Nanostructures: Magnetically Recoverable and Reusable Catalysts with High Activities. *J. Mater. Chem.* **2011**, *21*, 4904−4917.
(54) Juárez, J.; Cambón, A.; Goy-López, S.; Topete, A.; Taboada, P.; Mosquera, V. Obtention of Metallic Nanowires by Protein

Biotemplating and Their Catalytic Application. *J. Phys. Chem. Lett.* **2010**, *1*, 2680−2687.
(55) Thathagar, M. B.; Beckers, J.; Rothenberg, G. Copper-Catalyzed Suzuki Cross-Coupling Using Mixed Nanocluster Catalysts. *J. Am. Chem. Soc.* **2002**, *124*, 11858−11859.
(56) Narayanan, R.; El-Sayed, M. A. Catalysis with Transition Metal Nanoparticles in Colloidal Solution: Nanoparticle Shape Dependence and Stability. *J. Phys. Chem. B* **2005**, *109*, 12663−12676.
(57) Molnár, Á. Efficient, Selective, and Recyclable Palladium Catalysts in Carbon-Carbon Coupling Reactions. *Chem. Rev.* **2011**, *111*, 2251−2320.
(58) Li, Y.; Boone, E.; El-Sayed, M. A. Size Effects of PVP−Pd Nanoparticles on the Catalytic Suzuki Reactions in Aqueous Solution. *Langmuir* **2002**, *18*, 4921−4925.
(59) Kim, S.-J.; Oh, S.-D.; Lee, S.; Choi, S.-H. Radiolytic Synthesis of Pd-M (M = Ag, Ni, and Cu)/C Catalyst and Their Use in Suzuki-Type and Heck-Type Reaction. *J. Ind. Eng. Chem.* **2008**, *14*, 449−456.
(60) Kim, M.-R.; Choi, S.-H. One-Step Synthesis of Pd-M/ZnO (M═Ag, Cu, and Ni) Catalysts by γ-Irradiation and Their Use in Hydrogenation and Suzuki Reaction. *J. Nanomater.* **2009**, 302919:1−302919:7.
(61) Bradford, M. M. A Rapid and Sensitive Method for the Quantitation of Microgram Quantities of Protein Utilizing the Principle of Protein-Dye Binding. *Anal. Biochem.* **1976**, *72*, 248−254.